$SE(n)++$: An Efficient Solution to Multiple Pose Estimation Problems

Jin Wu, *Member, IEEE*, Ming Liu, *Senior Member, IEEE*, Yulong Huang, *Member, IEEE,* Chi Jin, Yuanxin Wu, *Senior Member, IEEE* and Changbin Yu, *Senior Member, IEEE*

***Abstract*—In robotic applications, many pose problems involve solving the homogeneous transformation based on the special Euclidean group $SE(n)$. However, due to the non-convexity of $SE(n)$, many of these solvers treat rotation and translation separately and the computational efficiency is still unsatisfactory. A new technique called the $SE(n)++$ is proposed in this paper that exploits a novel mapping from $SE(n)$ to $SO(n+1)$. The mapping transforms the coupling between rotation and translation into a unified formulation on the Lie group and gives better analytical results and computational performances. Specifically, three major pose problems are considered in this paper, i.e. the point-cloud registration, the hand-eye calibration and the $SE(n)$ synchronization. Experimental validations have confirmed the effectiveness of the proposed $SE(n)++$ method in open datasets.**

***Index Terms*—Pose Estimation, Point-Cloud Registration, Hand-eye Calibration, $SE(n)$ Synchronization**

I. Introduction

A. Motivations

ACCURATE robotic navigation, mapping and control require precision pose estimation from multiple kinds of measurements, which mostly comprise the visual, inertial and laser-scan data from heterogeneous sensors [1], [2]. Pose estimation is also important for human motion tracking and video analysis, which may be achieved via deep learning techniques [3], [4]. The pose referred to in this paper means the homogeneous transformation that contains both rotation and translation. The pose estimation problems in this paper mainly cover:

1) Point-cloud registration (PCR): Estimate the optimal rigid transformation between two noisy point clouds. It is rather useful for pose estimation from sensors like camera and laser scanners.
2) Hand-eye calibration (HEC): Estimate the extrinsic parameter between the robotic gripper (hand) and the attached camera (eye). Extended HEC also simultaneously computes the gripper-camera pose and the robot-world pose.
3) $SE(n)$ synchronization: Estimate the optimal pose sequence, provided that some relative transformations between them are known. It is a basic technique for pose refinement in simultaneous localization and mapping (SLAM), such as the pose-graph optimization (PGO).

Each of them has been extensively studied in the robotics community and even has received wide industrial applications. Since there are various frame transforms, some pose estimation problems may be highly non-convex [5]–[7]. Then the global searching will undergo long periods to converge to a satisfactory solution, such as the $SE(n)$ synchronization. Moreover, internal coupling mechanisms of rotation and translation also add up such non-convexity in practice.

The main contribution presented in this paper is that, a novel pose representation tool has been developed. It follows a simple mapping from the special Euclidean group $SE(n)$ to the special orthogonal group $SO(n+1)$, which will cast previous sophisticated problems into refined ones with rotation optimization only. The designed scheme is thus named as the $SE(n)$++ technique. The major advantages of the $SE(n)$++ are

1) It may deal with many kinds of homogeneous pose estimation problems e.g. PCR, HEC and $SE(n)$ synchronization.
2) It reduces the pose estimation to high-order rotation estimation, and the computational efficiency is significantly improved.
3) It combines rotation and translation in a unified form and thus the coupling of them are fully considered, which leads to simultaneous optimal estimation of the two parts.

The proposed $SE(n)$++ theory is based on the classical Lie theory and does not require extended motion parameterization theory. The rotation-matrix based form of $SE(n)++$ also makes it neat and intuitive when invoked for pose estimation.

Manuscript received X X, 20XX; revised X X, 20XX; accepted X X, 20XX. Date of publication X X, 20XX; date of current version X X, 20XX. Recommended by Technical Editor X X. This research was supported by the Open Project of Shanghai Key Laboratory of Navigation and Location-Based Services, Shanghai Jiao Tong University, in part by General Research Fund of Research Grants Council Hong Kong,11210017, and also in part by Early Career Scheme Project of Research Grants Council Hong Kong, 21202816. (*Corresponding author: Ming Liu*)

J. Wu and M. Liu are with Department of Electronic and Computer Engineering, Hong Kong University of Science and Technology, Hong Kong, China. (e-mail: jin_wu_uestc@hotmail.com; eelium@ust.hk)

Y. Huang is with School of Automation, Harbin Engineering University, Harbin, China and is also with Department of Electronic and Computer Engineering, City University of Hong Kong, Hong Kong, China. (e-mail: heuedu@163.com)

C. Jin is with DJI Innovation Inc., Shenzhen, China. (e-mail: chi.jin@uwaterloo.ca)

Y. Wu is with the Shanghai Key Laboratory of Navigation and Location-based Services, School of Electronic Information and Electrical Engineering, Shanghai Jiao Tong University, Shanghai, China (e-mail: yuanx_wu@hotmail.com)

C. Yu is with the School of Engineering, Westlake University, Hangzhou, China, and also with the Optus-Curtin Centre of Excellence in Artificial Intelligence, Curtin University, Perth, WA, Australia. (e-mail: yu@westlake.edu.cn)

Color versions of one or more of the figures in this paper are available online at http://ieeexplore.ieee.org.

It is noted that we aim at solving deterministic pose estimation problems i.e. the unknown correspondences using matching and learning techniques are regarded as resolved issues.

B. Related Works

1) Point-Cloud Registration: Since 1980s, with the rapid development of industrial visual instruments, the PCR has become practical in 3-D reconstruction. Arun et al. established the optimal theory of rigid pose estimation from two point clouds using singular value decomposition (SVD) in 1987 [8]. The classical PCR can only deal with the registration of two point clouds with the same dimension. When it comes to the reality, there is no guarantee of such requirement. The iterative closest point (ICP) has then been invented to iteratively find the best pose by matching the two point clouds with outlier rejection [9], [10]. ICP optimization is not convex in general and recently many efficient variants have been developed to give globally optimal estimates based on geometric analysis of $SE(3)$ or the branch-and-bound (BnB) strategy [11], [12].

PCR has revealed a very basic relationship between point correspondences. Therefore, it is potentially useful for some advanced pose estimation problems. For instance, in the effective perspective-n-point (EPnP) algorithm [13], the camera pose estimation problem has been solved via the PCR. An early study by Park et al. also shows the feasibility of the PCR for solution of hand-eye calibration [14]. PCR has also recently been employed for the time-offset determination between asynchronous visual and inertial measurements [15]. In theory, PCR owns almost the same structure as the Wahba's problem for spacecraft attitude determination [16]. As PCR is highly related to many other problems, it will be treated in this paper as the first introductory example for extension to other sophisticated problems.

2) Hand-eye Calibration: Shiu et al. were the first endeavors to develop the HEC between the robot gripper and camera [17]. They convert the HEC problem into a mathematical form of the type $\boldsymbol{AX} = \boldsymbol{XB}$ with $\boldsymbol{A}, \boldsymbol{B}$ known and $\boldsymbol{X}$ the unknown extrinsic parameter [18]. Almost at the same time, this technique has also been studied by Tsai in a quite different approach [19]. Early researches on the HEC focus on solving the problem analytically via different pose parameters like quaternion, dual quaternion, screw parameters and etc. [20]–[22]. Besides, a new framework of HEC has been proposed by Zhuang et al. that formulates the relationship of the type $\boldsymbol{AX} = \boldsymbol{YB}$ where $\boldsymbol{X}$ the gripper-camera transformation, $\boldsymbol{Y}$ the robot-world transformation are to be figured out with the known poses $\boldsymbol{A}$ and $\boldsymbol{B}$ [23]. It is pointed out in [14] that, apart from some special cases, general $\boldsymbol{AX} = \boldsymbol{XB}$ HEC problems are non-convex. Further study also shows the nonlinear coupling between the rotation and translation would be vital to the eventual accuracy for the type $\boldsymbol{AX} = \boldsymbol{YB}$ [24]. Thus the simultaneous solution of rotation and translation is a crucial problem. This leads to some developments for more accurate solutions using global optimization methods like Lie-group gradient descent (LGD) [25], alternate linear programming (ALP) [26], stochastic global optimization (SGO) [6], BnB [5] and etc. These algorithms have high complexity and thus are not suitable for real-time applications.

3) $SE(n)$ Synchronization: The PGO problem forms the key step in graph-based SLAM [27], [28], which is also very important for loop closure in the visual-inertial odometry (VIO) [29]. The PGO also has its application in localization of sensor networks with relative measurements [30], [31]. In mathematical research, the PGO problem is formulated as the $SE(n)$-Sync one i.e. only the relative transformations are known for the global estimation of poses for each vertex on the pose graph [32]. This is according to the fact that, in most circumstances, there is no a posteriori information of the nearby environment and only relative transformation can be acquired from successive keyframes. When the graph is in 2-D and contains few poses, the global optimization can be simply achieved via the direct Jacobian-based update [33], [34]. However, when the dimension increases, evaluating the Jacobian will consume huge load of time which may significantly affect the real-time performance. Carlone et al. have studied the diverse relaxation techniques for rotation optimization in PGO [35]. Carlone et al. also developed the 2-D PGO with guaranteed performance [36]. In a recent work, they paid more attention to the robust convex relaxation of 2-D PGO in the presence of outliers [37]. This work employs the maximum likelihood estimation (MLE) with probability density of Fisher-von-Mises (FVM) distribution (also called the Langevin distribution). This has been recently extended to the $SE(n)$ space by Rosen et al. where the semidefinite programming (SDP) on the Riemannian manifold has been invoked, such is called the SE-Sync algorithm [38]. Introducing a specific Cartan motion group, the Cartan-Sync algorithm aims to improve the computational efficiency of the SE-Sync [39]. However, Cartan-Sync inherits most characteristics of the SE-Sync, like to the Riemannian staircase. Thus the estimation is still sometimes time-consuming. The general pros and cons of these methods are summarized in Table I.

TABLE I
PROS AND CONS OF REPRESENTATIVE METHODS

• **R and t Separated (e.g. [14], [17], [19]–[24])**:
Pros: Computationally Efficient, Accurate when Measurement Noise Level is Low;
Cons: Not Optimal, Not Accurate when Measurement Noise Level is High.
• **R and t Coupled (e.g. [5], [6], [25], [26], [32], [37], [38])**:
Pros: Accurate;
Cons: Time-Consuming and Sometimes Hard to Converge

C. Organization of Our Works

Based on the aforementioned shortcomings of existing algorithms for multiple pose estimation problems, in the remainder of this paper, we introduce our new design of $SE(n)++$ in the Section II. The detailed solutions to the three main kinds of problems are then presented. The experimental evaluation and comparisons with representatives on various datasets are shown in Section III. The Section IV finally draws the concluding remarks and some future works.

II. PROPOSED $SE(n)++$ THEORY

A. Notations and Preliminaries

All n-dimensional rotation matrices belong to the special orthogonal group $SO(n) := \{\boldsymbol{R} \in \mathbb{R}^{n\times n} | \boldsymbol{R}^\top \boldsymbol{R} = \boldsymbol{I}, \det(\boldsymbol{R}) =$

$1\}$ where $\boldsymbol{I}$ denotes the identity matrix with proper size. The special Euclidean space is composed of a rotation matrix $\boldsymbol{R}$ and a translational vector $\boldsymbol{t}$ such that

$$SE(n) := \left\{ \boldsymbol{T} = \begin{pmatrix} \boldsymbol{R} & \boldsymbol{t} \\ \boldsymbol{0} & 1 \end{pmatrix} | \boldsymbol{R} \in SO(n), \boldsymbol{t} \in \mathbb{R}^n \right\} \quad (1)$$

with $\boldsymbol{0}$ denoting the zeros matrix with adequate dimensions. As $SO(n)$ belongs to the Lie group [40], the logarithmic mapping can be expressed by $\boldsymbol{x}_\times = \log \boldsymbol{R}$ where $\boldsymbol{x}_\times$ is the mapping from the $n(n-1)/2 \times 1$ vector $\boldsymbol{x}$ to the $n \times n$ dimensional skew-symmetric matrix as presented in (2) where $*$ denotes the skew symmetry.

$$\boldsymbol{x}_\times = \begin{pmatrix} 0 & -x_{\frac{n(n-1)}{2}} & x_{\frac{n(n-1)}{2}-1} & \cdots & (-1)^{n-2}x_{2n-3} & (-1)^{n-1}x_{n-1} \\ * & 0 & -x_{\frac{n(n-1)}{2}-2} & \cdots & (-1)^{n-3}x_{2n-4} & (-1)^{n-2}x_{n-2} \\ * & * & \ddots & \cdots & \vdots & \vdots \\ * & * & * & \ddots & -x_n & x_2 \\ * & * & * & * & 0 & -x_1 \\ * & * & * & * & * & 0 \end{pmatrix} \quad (2)$$

$\boldsymbol{x}$ here is called the Lie algebra of $\boldsymbol{R}$. The inverse of the $\times$ operator is denoted as $\wedge$ such that $\boldsymbol{x}_\times^\wedge = \boldsymbol{x}$. The inverse of the logarithmic mapping is the exponential mapping such that $e^{\log \boldsymbol{R}} = \boldsymbol{R}$. The operation $\mathrm{orthonormalize}$ denotes the orthonormalization of an arbitrary real square matrix.

B. $SE(n)++$ Mapping

The kernel innovation in this paper is that, the $SE(n)$ problems are mapped to the $SO(n+1)$ ones by means of

$$\boldsymbol{T} = \begin{pmatrix} \boldsymbol{R} & \boldsymbol{t} \\ \boldsymbol{0} & 1 \end{pmatrix} \underset{\mathcal{F}^{-1}}{\overset{\mathcal{F}}{\longleftrightarrow}} \boldsymbol{R}_{\boldsymbol{T},SO(n+1)} = \begin{pmatrix} \boldsymbol{R} & \varepsilon \boldsymbol{t} \\ -\varepsilon \boldsymbol{t}^\top \boldsymbol{R} & 1 \end{pmatrix} \quad (3)$$

in which ε denotes a tiny positive number for approximation on $SO(n+1)$. The mapping in (3) is called as the $SE(n)++$ for extending the $SE(n)$ transformation to the $SO(n+1)$ manifold. This formulation is based on the mapping from the $SE(3)$ to $SO(4)$ using the Caylay transform via the biquaternion dynamics [41]. The translation integration in (3) is different from that in [41] since our formulation achieves much better performance in practice (see our recent hand-eye calibration work [42]). In theory, the mapping from $SE(n)$ to $SO(n+1)$ is not unique and some nonlinear methods have been proposed [43]. Historically, the pose estimation problems on $SO(4)$ can be solved by either dual quaternions or double quaternions [44], [45]. However, when we generalize the problem on higher dimensional space $SO(n)$, these attitude parameterization approaches vanish. Therefore the proposed $SE(n)++$ problem is a novel one with mathematical challenges. (3) allows for the kinematics $\mathcal{F}(\boldsymbol{T}_1\boldsymbol{T}_2) = \mathcal{F}(\boldsymbol{T}_1)\mathcal{F}(\boldsymbol{T}_2)$ which coincides with the Lie group isomorphism. Note that the $\boldsymbol{R}_{\boldsymbol{T},SO(n+1)}$ in (3) is not strictly orthonormalized. Therefore, when taken into computation, $\boldsymbol{R}_{\boldsymbol{T},SO(n+1)}$ should be first orthonormalized to $SO(n+1)$, which can be achieved via the SVD. The inverse mapping $\mathcal{F}^{-1}$ aims to extract the optimal $\boldsymbol{R}$ and $\boldsymbol{t}$ from a coupled $SO(n+1)$ rotation matrix. Suppose the such rotation on $SO(n+1)$ can be written in the form of

$$\boldsymbol{R}_{SO(n+1)} = \begin{pmatrix} \boldsymbol{X} & \boldsymbol{x} \\ \boldsymbol{y}^\top & c \end{pmatrix} \quad (4)$$

Then the following relationship can be obtained

$$\begin{gathered} \mathrm{orthonormalize}(\boldsymbol{X}) = \boldsymbol{R} \\ \varepsilon \boldsymbol{t} = -\boldsymbol{R}\boldsymbol{y}, \ \varepsilon \boldsymbol{t} = \boldsymbol{x} \end{gathered} \quad (5)$$

Since ε is very small, we have $c \approx 1$, $\det(\boldsymbol{X}) \approx 1$. The least-square closed-form solution indicates that $\boldsymbol{t} = \frac{\boldsymbol{x} - \boldsymbol{R}\boldsymbol{y}}{2\varepsilon}$. The selection of ε in $SE(n)++$ is quite important. The strategy for choosing this parameter is empirical in the current study. The ε should be tiny enough to decrease the effect of orthonormalization but should not be too small to loose adequate word length. Then the following rule is applied to choose: $\varepsilon = \gamma / \|\boldsymbol{t}\|$ where $\gamma > 0$ is a scaling factor for the purpose shown above.

C. Uncertainty Descriptions of $SE(n)++$

The special orthogonal group $SO(n)$ is a subspace of the Stiefel manifold $\mathbb{S}^n$ that includes all the orthonormal matrices with determinant 1. Due to orthonormality constraint, the proper uncertain description of the matrices on Stiefel manifold can be given by the Fisher-von-Mises (FVM) or the Langevin distribution. A branch of the FVM is called the isotropic FVM distribution that can well characterize the probabilistic distribution of matrices on $SO(n)$, whose probability density function is given by

$$p(\boldsymbol{X}, \boldsymbol{M}, \kappa) = \frac{1}{c_n(\kappa)} \exp\left[\kappa \ \mathrm{tr}\left(\boldsymbol{M}^\top \boldsymbol{X}\right)\right] \quad (6)$$

with $\boldsymbol{M} \in SO(n)$ the mode i.e. the mean of $\boldsymbol{X}$ and $\kappa \geq 0$ the concentration parameter. $c_n(\kappa)$ plays an role of the probability normalization and is related to the dimension n. For instance, for $SO(2), SO(3)$, we have $c_2(\kappa) = I_0(2\kappa)$, $c_3(\kappa) = e^\kappa \left[I_0(2\kappa) - I_1(2\kappa)\right]$ where I_0, I_1 denote the modified Bessel functions of the first kind. Given a rotation variable $\boldsymbol{R}$ with mode $\boldsymbol{M}_{\boldsymbol{R}}$ and concentration parameter of $\kappa_{\boldsymbol{R}}$, combining with a translation $\boldsymbol{t} \sim \mathcal{N}(\boldsymbol{\mu}_{\boldsymbol{t}}, \boldsymbol{\Sigma}_{\boldsymbol{t}})$, we are able to give the following manipulations

$$\begin{aligned} & \boldsymbol{M}_{\boldsymbol{R}_{\boldsymbol{T},SO(n+1)}} = \begin{pmatrix} \boldsymbol{M}_{\boldsymbol{R}} & \varepsilon \boldsymbol{\mu}_{\boldsymbol{t}} \\ -\varepsilon \boldsymbol{\mu}_{\boldsymbol{t}}^\top \boldsymbol{M}_{\boldsymbol{R}} & 1 \end{pmatrix} \\ & \Rightarrow \mathrm{tr}\left(\boldsymbol{M}_{\boldsymbol{R}_{\boldsymbol{T},SO(n+1)}}^\top \boldsymbol{R}_{\boldsymbol{T},SO(n+1)}\right) \approx \mathrm{tr}\left(\boldsymbol{M}_{\boldsymbol{R}}^\top \boldsymbol{R}\right) + 1 \end{aligned} \quad (7)$$

This result reveals that the translation has very tiny impact on the probability density of the mapped rotation on $SO(n+1)$. This also indicates that the normalized FVM probability density function of the $SE(n)++$ is

$$p(\boldsymbol{X}, \boldsymbol{M}, \kappa) = \frac{1}{c_n(\kappa)\exp(\kappa)} \exp\left[\kappa \ \mathrm{tr}\left(\boldsymbol{M}^\top \boldsymbol{X}\right)\right] \quad (8)$$

where $\frac{1}{c_n(\kappa)\exp(\kappa)}$ acts as a new normalization factor for the derived probability density.

D. Generalized Homogeneous Pose Estimation

The homogeneous pose estimation allows for computing one pose or two poses from a set of equations of similar forms. Generally, any problem consisting of two unknown homogeneous poses can be formulated by $\boldsymbol{AX} = \boldsymbol{YB}$ with $\boldsymbol{A}, \boldsymbol{B} \in SE(n)$ known and $\boldsymbol{X}, \boldsymbol{Y}$ the unknown variables also on the $SE(n)$. Such type of equation can be utilized for multiple purposes as presented in Table II. We give the closed-form solution to these problems in the following contents.

TABLE II
SETUP OF DIFFERENT POSE ESTIMATION PROBLEMS

1) If $\boldsymbol{X} = \boldsymbol{I}$, the problem becomes the compressed point-cloud registration of the form $\boldsymbol{A} = \boldsymbol{YB}$.
2) If $\boldsymbol{X} = \boldsymbol{Y}$, the problem turns out to be the gripper-camera HEC of the type $\boldsymbol{AX} = \boldsymbol{XB}$.
3) If the variables hold their forms, the problem is cast to the simultaneous gripper-camera and robot-world HEC of the type $\boldsymbol{AX} = \boldsymbol{YB}$.
4) If $\boldsymbol{A} = \boldsymbol{I}$, the problem will be the $SE(n)$ synchronization that follows $\boldsymbol{X} = \boldsymbol{YB}$ where $\boldsymbol{B}$ is the known relative transformation between the unknown $\boldsymbol{X}$ and $\boldsymbol{Y}$.

The least-square estimation of $\boldsymbol{X}$ and $\boldsymbol{Y}$ is achieved by

$$\mathop{\arg\min}_{\boldsymbol{X}, \boldsymbol{Y} \in SE(n)} \sum_{i=1}^{N} w_i \left\| \boldsymbol{A}_i \boldsymbol{X} - \boldsymbol{Y} \boldsymbol{B}_i \right\|^2 \tag{9}$$

where $\boldsymbol{A}_i, \boldsymbol{B}_i$ are sequences of known i-th pair of transformations with relative positive weight w_i of the sum 1. The $SE(n)++$ mapping allows an equivalent form

$$\mathop{\arg\min}_{\boldsymbol{X}, \boldsymbol{Y} \in SO(n+1)} \mathcal{L} = \sum_{i=1}^{N} w_i \left\| \boldsymbol{A}_i \boldsymbol{X} - \boldsymbol{Y} \boldsymbol{B}_i \right\|^2 \tag{10}$$

with $\boldsymbol{A}_i, \boldsymbol{B}_i$ being mapped $SO(n+1)$ rotations from original transformations on $SE(n)$. The optimization loss function follows that

$$\begin{aligned} \mathcal{L} &= \sum_{i=1}^{N} w_i \ \mathrm{tr}\left[\left(\boldsymbol{A}_i \boldsymbol{X} - \boldsymbol{Y} \boldsymbol{B}_i \right)^\top \left(\boldsymbol{A}_i \boldsymbol{X} - \boldsymbol{Y} \boldsymbol{B}_i \right) \right] \\ &= 2N(n+1) - 2 \sum_{i=1}^{N} w_i \ \mathrm{tr}\left(\boldsymbol{X}^\top \boldsymbol{A}_i^\top \boldsymbol{Y} \boldsymbol{B}_i^\top \right) \end{aligned} \tag{11}$$

Let $\boldsymbol{\theta} = \left[\boldsymbol{\theta}_{\boldsymbol{X}}^\top, \boldsymbol{\theta}_{\boldsymbol{Y}}^\top \right]^\top$ where $\boldsymbol{\theta}_{\boldsymbol{X}} = (\log \boldsymbol{X})^\wedge$, $\boldsymbol{\theta}_{\boldsymbol{Y}} = (\log \boldsymbol{Y})^\wedge$, we have the Jacobian of $\mathcal{L}$ with respect to $\boldsymbol{\theta}$

$$\frac{\partial \mathcal{L}}{\partial \boldsymbol{\theta}} = -2 \sum_{i=1}^{N} w_i \frac{\partial \ \mathrm{tr}\left(\boldsymbol{X}^\top \boldsymbol{A}_i^\top \boldsymbol{Y} \boldsymbol{B}_i \right)}{\partial \boldsymbol{\theta}} \tag{12}$$

Some new matrix results are required to obtain the analytical form of the Jacobian, which are introduced herein.

For arbitrary squared matrices $\boldsymbol{A}$ and $\boldsymbol{B}$ with the same dimension of $\boldsymbol{\theta}_\times$, we have the following type of differentiation

$$\frac{\mathrm{d} \ \mathrm{tr}\left(\boldsymbol{A} \boldsymbol{\theta}_\times \boldsymbol{B} \right)}{\mathrm{d}\boldsymbol{\theta}} = \frac{\mathrm{tr}\left(\boldsymbol{A} \mathrm{d}\boldsymbol{\theta}_\times \boldsymbol{B} \right)}{\mathrm{d}\boldsymbol{\theta}} = \frac{\mathrm{tr}\left(\boldsymbol{B} \boldsymbol{A} \mathrm{d}\boldsymbol{\theta}_\times \right)}{\mathrm{d}\boldsymbol{\theta}} = \mathcal{Z}(\boldsymbol{BA}, n) \tag{13}$$

provided that the $\mathcal{Z}$ function is defined by $\mathcal{Z}(\boldsymbol{A}, n) = \mathrm{tr}[\boldsymbol{A} \ \mathrm{d}\boldsymbol{\theta}_\times] / \mathrm{d}\boldsymbol{\theta}$. In conclusion, we can obtain the compact form

$$\mathcal{Z}(\boldsymbol{A}, n) = \frac{\mathrm{tr}[\boldsymbol{A} \ \mathrm{d}\boldsymbol{\theta}_\times]}{\mathrm{d}\boldsymbol{\theta}} = \left(\boldsymbol{A}^\top - \boldsymbol{A} \right)^\wedge \tag{14}$$

Note that, for brevity, $\mathcal{Z}(\boldsymbol{A}, n)$ may be replaced by $\mathcal{Z}(\boldsymbol{A})$ where n is inferred from the dimension of $\boldsymbol{A}$. Then it follows that

$$\frac{\mathrm{d} \ \mathrm{tr}\left(\boldsymbol{A} \boldsymbol{\theta}_\times^p \right)}{\mathrm{d}\boldsymbol{\theta}} = \sum_{i=0}^{p-1} \mathcal{Z}\left(\boldsymbol{\theta}_\times^i \boldsymbol{A} \boldsymbol{\theta}_\times^{p-i-1} \right) \tag{15}$$

where the additivity of $\mathcal{Z}$ function is invoked, such that $\mathcal{Z}(\boldsymbol{A} + \boldsymbol{B}) = \mathcal{Z}(\boldsymbol{A}) + \mathcal{Z}(\boldsymbol{B})$. So it gives

$$\begin{aligned} &\frac{\mathrm{d} \ \mathrm{tr}\left[\left(\boldsymbol{\theta}_\times^p \right)^\top \boldsymbol{A} \boldsymbol{\theta}_\times^q \boldsymbol{B} \right]}{\mathrm{d}\boldsymbol{\theta}} = \frac{\mathrm{d} \ \mathrm{tr}\left[\boldsymbol{B} \left(\boldsymbol{\theta}_\times^p \right)^\top \boldsymbol{A} \boldsymbol{\theta}_\times^q \right]}{\mathrm{d}\boldsymbol{\theta}} \\ &= (-1)^p \frac{\mathrm{d} \ \mathrm{tr}\left(\boldsymbol{B} \boldsymbol{\theta}_\times^p \boldsymbol{A} \boldsymbol{\theta}_\times^q \right)}{\mathrm{d}\boldsymbol{\theta}} = (-1)^p \frac{\mathrm{tr}\left[\mathrm{d}\left(\boldsymbol{B} \boldsymbol{\theta}_\times^p \boldsymbol{A} \boldsymbol{\theta}_\times^q \right) \right]}{\mathrm{d}\boldsymbol{\theta}} \\ &= (-1)^p \ \mathcal{U}\left(\boldsymbol{B}, \boldsymbol{A}, p, q \right) \end{aligned} \tag{16}$$

with

$$\begin{aligned} &\mathcal{U}\left(\boldsymbol{A}, \boldsymbol{B}, p, q \right) := \frac{\mathrm{tr}\left[\mathrm{d}\left(\boldsymbol{A} \boldsymbol{\theta}_\times^p \boldsymbol{B} \boldsymbol{\theta}_\times^q \right) \right]}{\mathrm{d}\boldsymbol{\theta}} \\ &= \sum_{i=0}^{p-1} \mathcal{Z}\left(\boldsymbol{\theta}_\times^i \boldsymbol{B} \boldsymbol{\theta}_\times^q \boldsymbol{A} \boldsymbol{\theta}_\times^{p-i-1} \right) + \sum_{i=0}^{q-1} \mathcal{Z}\left(\boldsymbol{\theta}_\times^i \boldsymbol{A} \boldsymbol{\theta}_\times^p \boldsymbol{B} \boldsymbol{\theta}_\times^{q-i-1} \right) \end{aligned} \tag{17}$$

Since $e^{\boldsymbol{\theta}_\times} = \boldsymbol{I} + \boldsymbol{\theta}_\times + \frac{\boldsymbol{\theta}_\times^2}{2!} + \cdots$, defining

$$\mathcal{M}\left(\boldsymbol{A}, \boldsymbol{B}, p, q \right) := \sum_{j=0}^{p} \sum_{k=0}^{q} \frac{(-1)^j}{j!k!} \mathcal{U}\left(\boldsymbol{B}, \boldsymbol{A}^\top, j, k \right) \tag{18}$$

the closed form of the Jacobian when $\boldsymbol{X} = \boldsymbol{Y}$ is

$$\frac{\partial \mathcal{L}}{\partial \boldsymbol{\theta}} = -2 \sum_{i=1}^{N} w_i \mathcal{M}\left(\boldsymbol{A}_i, \boldsymbol{B}_i, p, q \right) \tag{19}$$

where $\boldsymbol{\theta} = (\log \boldsymbol{X})^\wedge$ and p, q are maximum order of the matrix exponentials. For (12), it is able to construct the following function based on the form of $\mathcal{U}$:

$$\begin{aligned} &\tilde{\mathcal{U}}\left(\boldsymbol{A}, \boldsymbol{B}, p, q \right) := \frac{\mathrm{tr}\left[\mathrm{d}\left(\boldsymbol{A} \boldsymbol{\theta}_{\boldsymbol{X},\times}^p \boldsymbol{B} \boldsymbol{\theta}_{\boldsymbol{Y}\times}^q \right) \right]}{\mathrm{d}\boldsymbol{\theta}} \\ &= \begin{bmatrix} \sum_{i=0}^{p-1} \mathcal{Z}\left(\boldsymbol{\theta}_{\boldsymbol{X},\times}^i \boldsymbol{B} \boldsymbol{\theta}_{\boldsymbol{Y},\times}^q \boldsymbol{A} \boldsymbol{\theta}_{\boldsymbol{X},\times}^{p-i-1} \right) \\ \sum_{i=0}^{q-1} \mathcal{Z}\left(\boldsymbol{\theta}_{\boldsymbol{Y},\times}^i \boldsymbol{A} \boldsymbol{\theta}_{\boldsymbol{X},\times}^p \boldsymbol{B} \boldsymbol{\theta}_{\boldsymbol{Y},\times}^{q-i-1} \right) \end{bmatrix} \end{aligned} \tag{20}$$

Likewise, defining

$$\tilde{\mathcal{M}}\left(\boldsymbol{A}, \boldsymbol{B}, p, q \right) := \sum_{j=0}^{p} \sum_{k=0}^{q} \frac{(-1)^j}{j!k!} \tilde{\mathcal{U}}\left(\boldsymbol{B}, \boldsymbol{A}^\top, j, k \right) \tag{21}$$

we have

$$\frac{\partial \mathcal{L}}{\partial \boldsymbol{\theta}} = -2 \sum_{i=1}^{N} w_i \tilde{\mathcal{M}}\left(\boldsymbol{A}_i, \boldsymbol{B}_i, p, q \right) \tag{22}$$

Then the local estimation of $\boldsymbol{\theta}$ can be achieved via the steepest descent algorithm

$$\boldsymbol{\theta}_k = \boldsymbol{\theta}_{k-1} - \gamma \frac{\partial \mathcal{L}}{\partial \boldsymbol{\theta}_{k-1}} \tag{23}$$

in which $\gamma > 0$ denotes the descending step length and k is the iteration index.

E. Maximum Likelihood Estimation

The maximum likelihood estimation (MLE) aims to give the optimal estimates based on the probability density functions of the measurements. Given N pairs of $\boldsymbol{A}_i, \boldsymbol{B}_i$ with associated rotation concentration parameter of κ_i, the likelihood function is expressed as follows

$$p\left(\boldsymbol{X}, \boldsymbol{Y}\right) = \prod_{i=1}^{N} \frac{\exp\left[\kappa_i \ \mathrm{tr}\left(\boldsymbol{X}^\top \boldsymbol{A}_i^\top \boldsymbol{Y} \boldsymbol{B}_i\right)\right]}{c_n(\kappa_i)\exp(\kappa_i)} \tag{24}$$

It is noticed that here the likelihood function is differentiable according to the fact that $SO(n+1)$ space is compact and smooth [46]. Defining the negative-logarithm-likelihood function $\mathcal{J}(\boldsymbol{\theta}) = -\log \ p\left(\boldsymbol{X}, \boldsymbol{Y}\right)$ the optimum meets

$$\frac{\partial \mathcal{J}}{\partial \boldsymbol{\theta}} = \boldsymbol{0} \Rightarrow \frac{\partial \mathcal{J}}{\partial \boldsymbol{\theta}} = -\sum_{i=1}^{N} \kappa_i \frac{\partial \mathrm{tr}\left(\boldsymbol{X}^\top \boldsymbol{A}_i^\top \boldsymbol{Y} \boldsymbol{B}_i\right)}{\partial \boldsymbol{\theta}} \tag{25}$$

which coincides with the least-square estimation shown in (12). That is to say, the least-square estimation also corresponds to the optimal probabilistic solution. Therefore, the uncertainty descriptions of $\boldsymbol{X}, \boldsymbol{Y}$ can be precisely obtained by computing the inverse of the Hessian of $\mathcal{J}$. Note that commonly MLE algorithms suffer from overfitting problems. It is commonly feasible to include regularization, maximum a posterior (MAP) estimation to overcome such problem. In the presented pose estimation problems, there is no such an overfitting problem since the relationship between the data and optimization target is deterministic which means the less the loss function is, the better the pose will be. Also note that a case of multiple solutions does not exist for $N \geq 2$, which has been shown in [6] and [22].

A new computationally efficient strategy is presented as follows. First, we need to guarantee that the solution is close to the true value i.e. the global optimum. The following procedure is performed for the global optimum searching. For the problem $\boldsymbol{AX} = \boldsymbol{YB}$, if we obtain an approximated solutions $\boldsymbol{X}_g, \boldsymbol{Y}_g$ using the g as the maximum orders of p and q, we can conduct the following manipulations:

$$\boldsymbol{AX} = \boldsymbol{YB} \Rightarrow \begin{cases} \boldsymbol{AX}\boldsymbol{X}_g^{-1} = \boldsymbol{YB}\boldsymbol{X}_g^{-1} \\ \quad \Rightarrow \boldsymbol{Y}_g^{-1}\boldsymbol{AX}\boldsymbol{X}_g^{-1} = \boldsymbol{Y}_g^{-1}\boldsymbol{YB}\boldsymbol{X}_g^{-1} \end{cases} \tag{26}$$

Now using $\tilde{\boldsymbol{A}} = \boldsymbol{Y}_g^{-1}\boldsymbol{A}$, $\tilde{\boldsymbol{X}} = \boldsymbol{X}\boldsymbol{X}_g^{-1}$, $\tilde{\boldsymbol{Y}} = \boldsymbol{Y}_g^{-1}\boldsymbol{Y}$ and $\tilde{\boldsymbol{B}} = \boldsymbol{B}\boldsymbol{X}_g^{-1}$, since $\boldsymbol{X}_g, \boldsymbol{Y}_g$ approximate $\boldsymbol{X}, \boldsymbol{Y}$ respectively, $\tilde{\boldsymbol{X}}$ and $\tilde{\boldsymbol{Y}}$ will be closer to the identity matrix $\boldsymbol{I}$. The new task will be the induced $\tilde{\boldsymbol{A}}\tilde{\boldsymbol{X}} = \tilde{\boldsymbol{Y}}\tilde{\boldsymbol{B}}$. By recursively doing so, the norm of $\boldsymbol{\theta}$ will be very tiny and the required maximum orders of p and q can be very small to reach the desired accuracy. The similar technique also applies to the problem $\boldsymbol{AX} = \boldsymbol{XB}$. Since $\tilde{\boldsymbol{X}}$ and $\tilde{\boldsymbol{Y}}$ are close to $\boldsymbol{I}$ after several iterations, their Lie algebra $\boldsymbol{\theta}_{\tilde{\boldsymbol{X}}}$ and $\boldsymbol{\theta}_{\tilde{\boldsymbol{Y}}}$ will be close to $\boldsymbol{0}$. In such condition, the Hessian $\boldsymbol{H}$ of $\mathcal{J}$ can be precisely restored by the first-order approximation of matrix exponentials, such that

$$\boldsymbol{H} = \frac{\partial^2 \mathcal{J}}{\partial \boldsymbol{\theta}^2} \approx -\sum_{i=1}^{N} \kappa_i \frac{\partial^2 \ \mathrm{tr}\left(\boldsymbol{\theta}_{\tilde{\boldsymbol{X}},\times}^\top \tilde{\boldsymbol{A}}_i^\top \boldsymbol{\theta}_{\tilde{\boldsymbol{Y}},\times} \tilde{\boldsymbol{B}}_i\right)}{\partial \boldsymbol{\theta}^2} \tag{27}$$

where $\tilde{\boldsymbol{A}}_i$, $\tilde{\boldsymbol{B}}_i$ are equivalent matrices coming from the manipulation in (26). For instance, when the error angle is 10° i.e. 0.17453 rad, the equivalent approximation rate is $(1 + 0.17453)/\exp(0.17453) = 98.64\%$ and for 5° it reaches 99.64%. The closed-form of $\boldsymbol{H}$ can be given by the following differentiation

$$\frac{\partial}{\partial \boldsymbol{\theta}} \frac{\partial \ \mathrm{tr}\left(\boldsymbol{A}\boldsymbol{\theta}_{\boldsymbol{X},\times}\boldsymbol{B}\boldsymbol{\theta}_{\boldsymbol{Y},\times}\boldsymbol{C}\right)}{\partial \boldsymbol{\theta}} = \begin{bmatrix} \mathcal{Z}\left(-\boldsymbol{B}\boldsymbol{\theta}_{\boldsymbol{Y},\times}^\top \boldsymbol{C}\boldsymbol{A}, n\right) \\ \mathcal{Z}\left(-\boldsymbol{B}^\top \boldsymbol{\theta}_{\boldsymbol{X},\times}^\top \boldsymbol{A}^\top \boldsymbol{C}^\top, n\right) \end{bmatrix} \tag{28}$$

Thus

$$\begin{aligned} &\frac{\partial^2 \ \mathrm{tr}\left(\boldsymbol{A}\boldsymbol{\theta}_{\boldsymbol{X},\times}\boldsymbol{B}\boldsymbol{\theta}_{\boldsymbol{Y},\times}\boldsymbol{C}\right)}{\partial \boldsymbol{\theta}^2} \\ &= \begin{bmatrix} \frac{\partial \mathcal{Z}^\top\left(-\boldsymbol{B}\boldsymbol{\theta}_{\boldsymbol{Y},\times}^\top \boldsymbol{C}\boldsymbol{A}, n\right)}{\partial \boldsymbol{\theta}_{\boldsymbol{X}}} & \frac{\partial \mathcal{Z}^\top\left(-\boldsymbol{B}\boldsymbol{\theta}_{\boldsymbol{Y},\times}^\top \boldsymbol{C}\boldsymbol{A}, n\right)}{\partial \boldsymbol{\theta}_{\boldsymbol{Y}}} \\ \frac{\partial \mathcal{Z}^\top\left(-\boldsymbol{B}^\top \boldsymbol{\theta}_{\boldsymbol{X},\times}^\top \boldsymbol{A}^\top \boldsymbol{C}^\top, n\right)}{\partial \boldsymbol{\theta}_{\boldsymbol{X}}} & \frac{\partial \mathcal{Z}^\top\left(-\boldsymbol{B}^\top \boldsymbol{\theta}_{\boldsymbol{X},\times}^\top \boldsymbol{A}^\top \boldsymbol{C}^\top, n\right)}{\partial \boldsymbol{\theta}_{\boldsymbol{Y}}} \end{bmatrix} \\ &= \begin{bmatrix} \boldsymbol{0} & \mathcal{D}_{\mathcal{Z}}\left(-\boldsymbol{B}, \boldsymbol{C}\boldsymbol{A}\right) \\ \mathcal{D}_{\mathcal{Z}}\left(-\boldsymbol{B}^\top, \boldsymbol{A}^\top \boldsymbol{C}^\top\right) & \boldsymbol{0} \end{bmatrix} \end{aligned} \tag{29}$$

which belongs to the following type

$$\mathcal{D}_{\mathcal{Z}}(\boldsymbol{A}, \boldsymbol{B}) = \frac{\partial \mathcal{Z}^\top\left(\boldsymbol{A}\boldsymbol{\theta}_\times^\top \boldsymbol{B}\right)}{\partial \boldsymbol{\theta}} = \frac{\mathcal{Z}^\top\left[\mathrm{d}\left(\boldsymbol{A}\boldsymbol{\theta}_\times^\top \boldsymbol{B}\right)\right]}{\mathrm{d}\boldsymbol{\theta}} \tag{30}$$

The internal differentiation is given by

$$\frac{\partial (\boldsymbol{A}\boldsymbol{\theta}_\times^\top \boldsymbol{B})_{ij}}{\partial \theta_k} = (-1)^k \left[A_{(i)(n)}B_{(n-k)(j)} - A_{(i)(n-k)}B_{(n)(j)}\right] \tag{31}$$

which finally gives the analytical form of $\boldsymbol{H}$ and thus presents the covariance of $\boldsymbol{\theta}$

$$\boldsymbol{\Sigma}_{\boldsymbol{\theta}\boldsymbol{\theta}} = \boldsymbol{H}^{-1} \tag{32}$$

The method for evaluating the covariance of the rotation and translation from $\boldsymbol{\theta}$ can be categorized into the high-dimensional registration problem, which is discussed in [47].

III. Experimental Results

In this section, three categories of experiments are conducted, including point-cloud registration, hand-eye calibration and $SE(n)$ synchronization problems. Different problems correspond to different situations shown in Table II. The general algorithm table of the proposed $SE(n)++$ method is shown in Algorithm 1. For the case of PCR, we use MATLAB on a MacBook Pro 2017 i7-3.5GHz laptop for computation and demonstration. For HEC problems, C++ programming language of standard 2011 has been utilized. For $SE(n)$ synchronization, C++ standard 2014 (C++14) is invoked for advanced features. Note that for $\boldsymbol{AX} = \boldsymbol{XB}$ HEC problem, various methods are implemented using on MacBook laptop while for $\boldsymbol{AX} = \boldsymbol{YB}$ one, algorithms are deployed on a

Algorithm 1 Algorithmic procedures of proposed $SE(n)$++.

1. Preparation: From Table II, select the problem type and then prepare matrices $\boldsymbol{A}_i, \boldsymbol{B}_i$ for $i = 1, 2, \cdots, N$. Determine an adequate parameter ε for $SE(n)$++ and a proper gradient-descent step length γ.
2. Conduct $SE(n)++$ **Mapping**: Map all matrices $\boldsymbol{A}_i, \boldsymbol{B}_i$ for $i = 1, 2, \cdots, N$ from $SE(n)$ space to $SO(n+1)$ space using (3).
3. Gradient Descent: Perform gradient descent searching using Lie-algebra formulae (12)-(23).
4. Global Refinement: Transform the problem using (26) to find the global optimum.
5. Inverse $SE(n)++$ **Mapping**: Once the global optimum is reached, map all solutions $\boldsymbol{X}$ and $\boldsymbol{Y}$ back from $SO(n+1)$ to $SE(n)$ using (3).

mobile computer on an unmanned aerial vehicle. Codes of the proposed $SE(n)++$ transform will be accessible at `https://github.com/zarathustr/SEnpp`.

A. Point-Cloud Registration

The open-source KITTI dataset is employed for validation of PCR [48]. We use the laser-scan measurements logged in this dataset from the Velodyne HDL-64E 64-beam rotating 3D laser scanner. The serial number of the dataset is `2011_09_29_drive_0071_sync`. The 57-th and 58-th laser scans are taken for rigid registration using the ICP. The ICP utilized here consists of the initial rotation guess of identity matrix, the matching strategy of kd tree and multiple rigid pose estimation kernels using representatives including SVD, eigen-decomposition (EIG), fast symbolic 3-D registration (FS3R), fast analytical 3-D registration (FA3R) and the proposed $SE(n)++$. The rigid transformation between the two scans has been estimated by these different algorithms. The results of the $SE(n)++$ are shown in Fig. 1, where the ε has been determined by the empirical law. Convergence rates of the selected five kernels are shown jointly in Fig. 2.

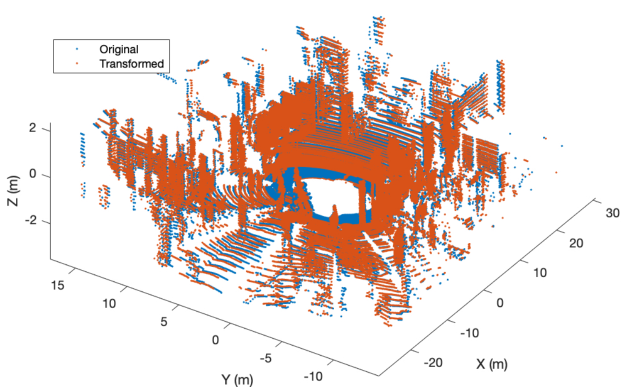

Fig. 1. The scene registration using $SE(n)++$ with KITTI dataset.

In Fig. 1, the 'original' one indicates the 57-th scan while the 'transformed' is the restored one from 58-th one using the obtained rigid transformation. The 3-D points of the two successive scans are well matched and the $SE(n)++$ also

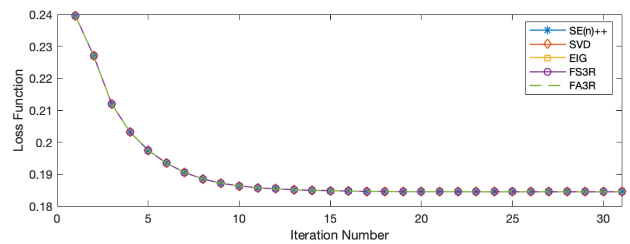

Fig. 2. The convergence rates of ICP with multiple kernels.

achieves the same convergence rate and final accuracy as that of other representatives. This indicates the correctness of the $SE(n)++$ for PCR problem.

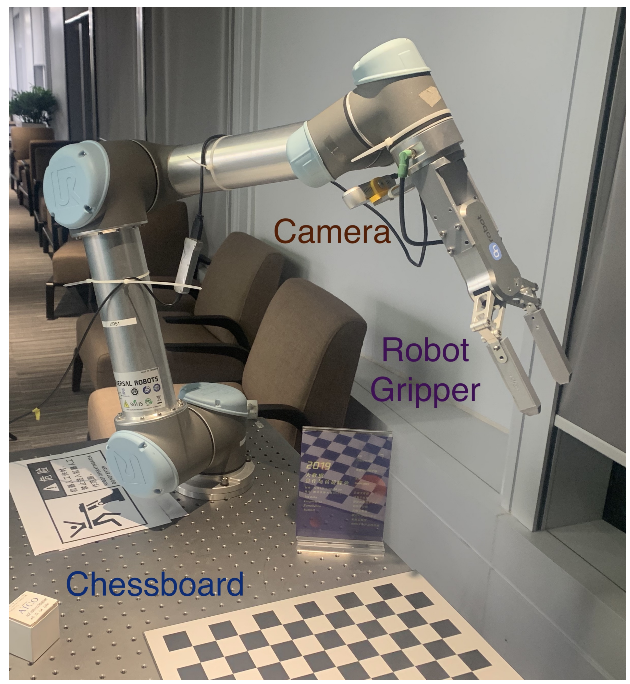

Fig. 3. The industrial hand-eye calibration setup.

B. Hand-eye Calibration

First, an industrial HEC problem is considered. The experimental setup is shown in Fig. 3. A UR5 industrial robot is utilized as the robotic manipulator. An Intel Realsense D435i camera is firmly attached to the robot. There is also a robot gripper installed on the robot aiming to conduct precision grasping tasks. HEC problem considers estimating relative extrinsic parameter between camera and robot gripper so the frames of camera and gripper can be aligned. To perform HEC operations, relative motions must be generated. We estimate the camera pose by using a 12x9 chessboard on the table. Several algorithms reviewed in the Introduction part are compared, including method of Tsai [19] and the BnB method [5]. We evaluate various algorithms by the root mean squared error (RMSE) of the mean loss function

$$\mathrm{RMSE} = \sqrt{\frac{1}{N}\sum_{i=1}^{N} \|\boldsymbol{A}_i\boldsymbol{X} - \boldsymbol{X}\boldsymbol{B}_i\|^2} \tag{33}$$

20 repeated calibration tasks are conducted using the experimental platform. We compute the mean RMSE values using these 20 cases. The results are shown in Table III. One may

TABLE III
RMSEs OF VARIOUS ALGORITHM FOR HAND-EYE CALIBRATION $\boldsymbol{AX} = \boldsymbol{XB}$ (AVERAGED)

Algorithms	RMSE
Proposed $SE(n)++$	0.16922
Tsai [19]	0.33281
BnB [5]	0.16923

observe that the proposed $SE(n)++$ method can estimate the hand-eye parameter $\boldsymbol{X}$ with high accuracy. Tsai's method is analytical one so it can not solve the nonlinear coupling between $\boldsymbol{R}$ and $\boldsymbol{t}$ in $\boldsymbol{X}$. The BnB method has been regarded as a highly accurate one in industrial processing. Thus the results verify that $SE(n)++$ is capable of dealing with such HEC problems.

Next, the robot-world/hand-eye calibration problem $\boldsymbol{AX} = \boldsymbol{YB}$ is deployed for experimental study. A DJI S800-EVO hexarotor unmanned air vehicle (HUAV) is used as the general carrying platform (see Fig. 4). This HUAV integrates a DJI Zenmuse Z15 gimbal that stabilizes a high-resolution Sony NEX-7 camera. A fisheye camera is firmly installed to the body of the HUAV and all the data has been processed at 20Hz with an onboard Nvidia TX1 computer. The data transmission of the two cameras is synchronous in the hardware level. The HEC involved in this system is dynamic, i.e. it aims to dynamically compute the transformation between the fisheye and gimbaled camera. The gimbaled camera follows the motion by an automatic tracking applet on the TX1 computer and thus the pose to the fisheye camera is time-varying. The HUAV has been remotely operated by a 2.4GHz wireless transmitter and the gimbaled camera tracks one checkerboard in the experimental environment. The pose estimation of the gimbaled camera has been conducted via the EPnP algorithm [13]. For the fisheye camera, the pose estimation has been conducted via the ORB-SLAM algorithm [49]. Among many experiments, one section has been selected, whose camera poses are shown in Fig. 5. The ALP [26] and the SGO [6] have also been applied to solve the $\boldsymbol{AX} = \boldsymbol{YB}$ HEC problem and for $SE(n)++$ the ε is determined using the empirical law. The RMSE is defined as

$$\mathrm{RMSE} = \sqrt{\frac{1}{N}\sum_{i=1}^{N} \|\boldsymbol{A}_i\boldsymbol{X} - \boldsymbol{Y}\boldsymbol{B}_i\|^2} \tag{34}$$

In the problem $\boldsymbol{AX} = \boldsymbol{YB}$, the rotation and translation are highly coupled. An analytical solution to such problem has been conducted to give an initial guess and multiple iterative algorithms are invoked for global solutions, including methods like LGD [25], ALP [26] and SGO [6]. For the steepest descent algorithm, the step length γ has been chosen as $\gamma = 1 \times 10^{-3}$, which is the same for the gradient descent in LGD and SGO. The algorithms are implemented on the computer of the HUAV platform. The in-run statistics are summarized as follows in Table IV.

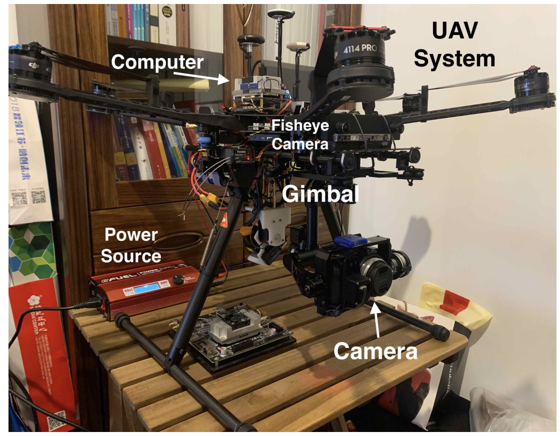

Fig. 4. The haxarotor platform for HEC of the type $\boldsymbol{AX} = \boldsymbol{YB}$.

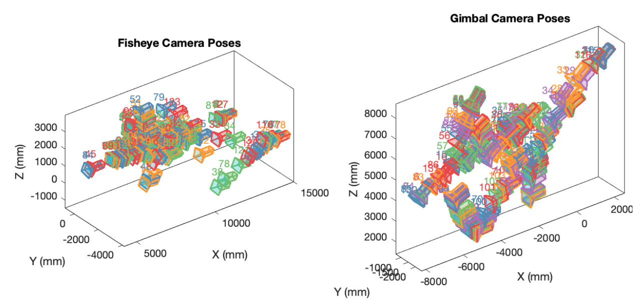

Fig. 5. The reconstructed poses from fisheye and gimbaled cameras.

The results show that the $SE(n)++$ method is able to reach the best performance of ALP among all algorithms. However, as ALP seeks the optimum via nonlinear programming, the consumed computational resources are much higher than that in $SE(n)++$, which is the common characteristic for other global solutions. The reason is that the designed solving process using $SE(n)++$ has neat form of the Jacobians and evaluating them can be much easier. Also, the manipulation in (26) allows the error converging with the rate on $SO(n+1)$, which also guarantees the accuracy.

C. $SE(n)$ Synchronization

The $SE(n)$ synchronization problem considers estimating N group elements on $SE(n)$ $\boldsymbol{X}_1, \boldsymbol{X}_2, \cdots, \boldsymbol{X}_N$, with given relative transformations $\boldsymbol{X}_{ij} = \boldsymbol{X}_i^{-1}\boldsymbol{X}_j$ for $i \neq j$. Such problem can be characterized by the following optimization

$$\mathop{\arg\min}_{\boldsymbol{X}_i \in SE(n)} \sum_{(i,j)\in\vec{\Upsilon}} w_{ij} \left\|\boldsymbol{X}_j - \boldsymbol{X}_{ij}\boldsymbol{X}_i\right\|^2, \quad i = 1, 2, \cdots, N \tag{35}$$

where $\vec{\Upsilon}$ denotes the edge of a directed graph describing the availability and directions of the relative transformations; w_{ij} denotes the weights of the connection (i,j) and could be given by the distribution of the relative transformation $\boldsymbol{X}_{ij}$, e.g. the Langevin distribution for uncertainty description of orthonormal matrices. By using the proposed $SE(n)++$

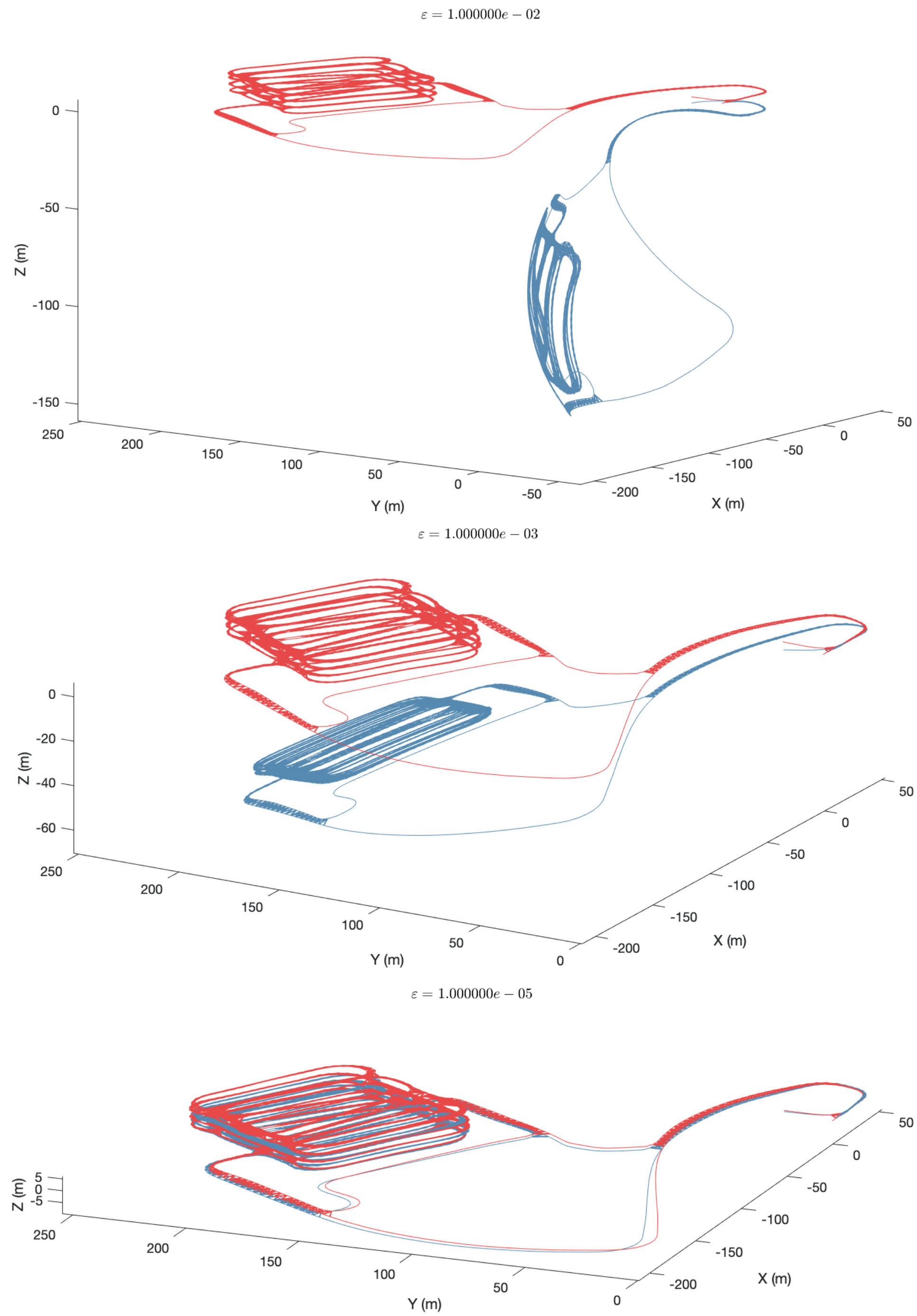

Fig. 6. The 3-D PGO results of `garage` with different values of ε.

technique, the new optimization is formulated as

$$\mathop{\arg\min}_{\boldsymbol{X}_i \in SO(n+1)} \sum_{(i,j)\in\vec{\Upsilon}} w_{ij} \left\| \boldsymbol{X}_j - \boldsymbol{X}_{ij,SO(n+1)} \boldsymbol{X}_i \right\|^2 \tag{36}$$

which can be directly solved via the rotation-only estimation

$$\mathop{\arg\min}_{\boldsymbol{X} \in SO(n+1)^N} \operatorname{tr}\left(\boldsymbol{Q}\boldsymbol{X}^\top \boldsymbol{X}\right) \tag{37}$$

with $\boldsymbol{X} = (\boldsymbol{X}_1, \boldsymbol{X}_2, \cdots, \boldsymbol{X}_N) \in SO(n+1)^N \subset \mathbb{R}^{(n+1)\times(n+1)N}$ and $\boldsymbol{Q}$ denotes the Laplacian matrix of the measurements $\boldsymbol{X}_{ij}$ whose details are given in [38]. Optimization (37) can be solved via the semidefinite programming in [38]. However, in [38], the rotation and translation parts of $SE(n)$ elements are independently solved and in fact the rotational and translational factors contribute to each other in the $SE(n)$ synchronization problem. The developed $SE(n)++$ problem can therefore couple the two effects together in the form of $SO(n+1)$ and the synchronization accuracy can be potentially increased. Another merit of the $SE(n)++$ for $SE(n)$ synchronization is that the computational efficiency has been significantly improved. The reason is that $SO(n)$

TABLE IV
RUN-TIME AND RMSE STATS OF VARIOUS ALGORITHM FOR ROBOT-WORLD/HAND-EYE CALIBRATION $\boldsymbol{AX} = \boldsymbol{YB}$ (AVERAGED)

Algorithms	RMSE	CPU Load	RAM Occupation
Proposed $SE(n)++$	0.08932	5.732%	31.79%
LGD [25]	0.13325	12.44%	39.82%
ALP [26]	0.08881	27.93%	38.80%
SGO [6]	0.09739	22.46%	34.16%

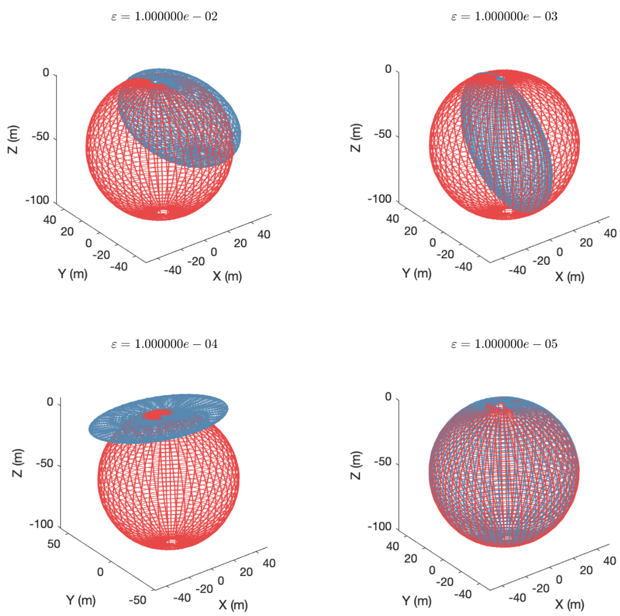

Fig. 7. The 3-D PGO results of `sphere` with different values of ε.

manifold has higher convexity than the $SE(n)$ manifold. Therefore, when solving such problem using the SDP, $SO(n)$ method will show much faster convergence. It is also noted that, the convergent gradient-descent optimizer on $SO(3)$ has also been well-developed [25]. The research on the convex hull of $SO(n)$ also verifies this point [50].

The open-source datasets of multiple pose graphs by Carlone et al. have been studied in this sub-section [32]. Three representatives i.e. `garage`, `sphere` and `city10000` are investigated. The `garage` originates from the 3-D SLAM test in the Stanford parking garage. The dataset `sphere` consists of relative poses over a 3-D spherical trajectory while `city1000` includes the information of the 2-D mapping in a city. The purpose of experimental studies in this sub-section is three-fold: 1) Understanding the effects of different selections of ε for $SE(n)++$; 2) Validate the effectiveness of the $SE(n)++$ with various dimensions n; 3) Study the superiority of the proposed $SE(n)++$ on computational efficiency. We use the SE-Sync [38] results as the reference where the parameters are consistent with the original one in [38]. The details are shown in the red color in the following figures. In contrast, The pose reconstruction results of the $SE(n)++$ are presented in the color of blue. First, let us see the performances of the $SE(n)$ synchronization in Fig. 6. There are three values for ε ranging from 10^{-2} to 10^{-5}. From the first two sub-figures, we are able to observe that, for large

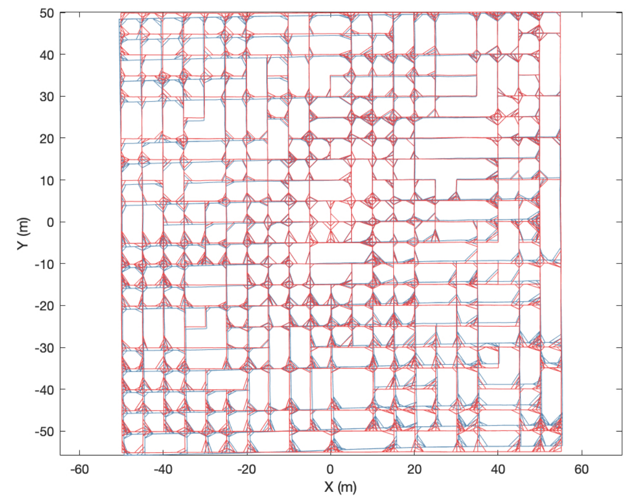

Fig. 8. The 2-D PGO results of `city10000` with $\varepsilon = 1 \times 10^{-6}$.

TABLE V
COMPUTATIONAL EFFICIENCY OF POSE-GRAPH OPTIMIZATION FOR DIFFERENT ALGORITHMS

3-D Datasets	TORO	SE-Sync	Cartan-Sync	Proposed $SE(n)++$
`sphere`	6.92s	4.79s	7.55s	**1.95**s
`torus`	12.77s	9.31s	6.18s	**3.10**s
`grid`	57.83s	43.94s	22.32s	**9.98**s
`garage`	18.26s	12.93s	19.3s	**1.065**s
`cubicle`	24.70s	12.66s	18.13s	**3.59**s
`rim`	68.41s	42.12s	47.19s	**9.13**s
2-D Datasets	TORO	SE-Sync	Cartan-Sync	Proposed $SE(n)++$
`CSAIL`	4.53s	3.32s	1.29s	1.76s
`manhattan`	9.32s	9.20s	2.76s	4.53s
`city10000`	12.24s	12.35s	14.96s	**5.34**s
`intel`	4.06s	3.18s	2.38s	**1.31**s
`ais`	233.9s	169.4s	104.47s	**28.88**s

ε, the orthonormalization errors are also large, leading to the incomplete descriptions of the rotation-translation coupling. When ε continuously decreases to 10^{-5}, the $SE(n)++$ can well model the pose so the results are quite accurate. The same behaviour also repeats for the `sphere` dataset, which is shown in Fig. 7. The sphere is able to be recovered very close to the reference when ε reaches a relatively small value. This shows that, adequate selection of ε leads to complete descriptions of rotation and translation by the proposed $SE(n)++$.

The computational efficiency have been compared with recent representatives including the TORO [33], SE-Sync [38] and Cartan-Sync [39]. We compare all the algorithms on the laptop appeared in the Section III.A and the methods are implemented using the C++ programming language with standard C++14 with support of `g2o` and `eigen` libraries, compiled with the `apple-darwin clang-1000.11.45.5` compiler where no optimization options have been enabled, which leads to non-parallelization of program execution and thus guarantees fairness of comparison. The run-time stats of various algorithms are shown in Table V. The results show that although $SE(n)++$ is not always the best one, it achieves fast computation speed for all 3-D cases and most 2-D cases. This is because the convexity of $SO(n+1)$ is still simpler than that of the $SE(n)$. As $SE(n)$ couples $\boldsymbol{R}$ and $\boldsymbol{t}$ separately, the global searching will require more computational resources. The advance in the computation time can enhance the real-time performance of the in-run robotic PGO. For graph-based SLAM, with the increasing dimension of the pose graph, the complexity catastrophe becomes more and more serious. The proposed $SE(n)++$ method can then give an effective way for balancing the accuracy and execution time.

D. Discussion

From the experimental results presented above, we may see that the proposed $SE(n)++$ mapping is effective for related pose estimation problems. In particular, it transforms original $SE(n)$ problems into those on $SO(n+1)$ and thus makes the new problems much easier to solve. As shown in Table IV and V, the computational efficiency has been significantly improved while the developed method reaches good accuracy for pose reconstruction as shown in Fig. 6 to Fig. 8. Results for solving real-world industrial HEC problems also show that the proposed $SE(n)++$ method is capable of decoupling $\boldsymbol{R}$ and $\boldsymbol{t}$ in a computationally efficient manner.

IV. Conclusion

A new mapping called the $SE(n)++$ has been proposed in this paper that maps the homogeneous transformation on $SE(n)$ to the $SO(n+1)$. This technique allows for transforming previous highly nonlinear problems on $SE(n)$ into new ones on $SO(n+1)$ and thus decreases the difficulty of globally optimal searching. Neat generalized Lie algebra solutions for homogeneous pose estimation problems are derived and related uncertainty descriptions have been found out through the maximum likelihood estimation. The point-cloud registration, hand-eye calibration and $SE(n)$ synchronization problems are extensively studied in the experimental part. The final performances indicate that the newly developed $SE(n)++$ is not only feasible, but also quite computationally efficient, compared with recent important representatives. The $SE(n)++$ has provided a new perspective for the pose estimation. In future works, it is expected to be used for advanced control problems considering rotation and translation simultaneously.

References

[1] P. Miraldo, H. Araujo, and N. Goncalves, "Pose estimation for general cameras using lines," *IEEE Trans. Cybern.*, vol. 45, no. 10, pp. 2156–2164, 2015.

[2] O. Tahri, H. Araujo, Y. Mezouar, and F. Chaumette, "Efficient iterative pose estimation using an invariant to rotations," *IEEE Trans. Cybern.*, vol. 44, no. 2, pp. 199–207, 2014.

[3] M. C. Chang, L. Ke, H. Qi, L. Wen, and S. Lyu, "Fast Online Video Pose Estimation by Dynamic Bayesian Modeling of Mode Transitions," *IEEE Trans. Cybern.*, pp. 1–14, 2019.

[4] N. McLaughlin, J. Martinez-del Rincon, and P. Miller, "3-D Human Pose Estimation Using Iterative Conditional Squeeze and Excitation Networks," *IEEE Trans. Cybern.*, pp. 1–13, 2020.

[5] J. Heller, M. Havlena, and T. Pajdla, "Globally Optimal Hand-Eye Calibration Using Branch-and-Bound," *IEEE Trans. Pattern Anal. Mach. Intell.*, vol. 38, no. 5, pp. 1027–1033, 2016.

[6] J. Ha, D. Kang, and F. C. Park, "A Stochastic Global Optimization Algorithm for the Two-Frame Sensor Calibration Problem," *IEEE Trans. Ind. Electron.*, vol. 63, no. 4, pp. 2434–2446, 2016.

[7] A. Assa and F. Janabi-Sharifi, "Virtual Visual Servoing for Multicamera Pose Estimation," *IEEE/ASME Trans. Mechatronics*, vol. 20, no. 2, pp. 789–798, 2015.

[8] K. S. Arun, T. S. Huang, and S. D. Blostein, "Least-Squares Fitting of Two 3-D Point Sets," *IEEE Trans. Pattern Anal. Mach. Intell.*, vol. PAMI-9, no. 5, pp. 698–700, 1987.

[9] P. J. Besl and N. D. McKay, "A Method for Registration of 3-D Shapes," *IEEE Trans. Pattern Anal. Mach. Intell.*, vol. 14, no. 2, pp. 239–256, 1992.

[10] F. Aghili and C.-Y. Su, "Robust Relative Navigation by Integration of ICP and Adaptive Kalman Filter Using Laser Scanner and IMU," *IEEE/ASME Trans. Mechatronics*, vol. 21, no. 4, pp. 2015–2026, 2016.

[11] A. Parra Bustos, T. J. Chin, A. Eriksson, H. Li, and D. Suter, "Fast Rotation Search with Stereographic Projections for 3D Registration," *IEEE Trans. Pattern Anal. Mach. Intell.*, vol. 38, no. 11, pp. 2227–2240, 2016.

[12] J. Yang, H. Li, D. Campbell, and Y. Jia, "Go-ICP: A Globally Optimal Solution to 3D ICP Point-Set Registration," *IEEE Trans. Pattern Anal. Mach. Intell.*, vol. 38, no. 11, pp. 2241–2254, 2016.

[13] V. Lepetit, F. Moreno-Noguer, and P. Fua, "EPnP: An accurate O(n) solution to the PnP problem," *Int. J. Comput. Vis.*, vol. 81, no. 2, pp. 155–166, 2009.

[14] F. C. Park and B. J. Martin, "Robot Sensor Calibration: Solving AX = XB on the Euclidean Group," *IEEE Trans. Robot. Autom.*, vol. 10, no. 5, pp. 717–721, 1994.

[15] J. Kelly, N. Roy, and G. S. Sukhatme, "Determining the time delay between inertial and visual sensor measurements," *IEEE Trans. Robot.*, vol. 30, no. 6, pp. 1514–1523, 2014.

[16] J. Wu, M. Liu, Z. Zhou, and R. Li, "Fast Symbolic 3D Registration Solution," *IEEE Trans. Autom. Sci. Eng.*, 2019.

[17] Y. C. Shiu and S. Ahmad, "Calibration of Wrist-Mounted Robotic Sensors by Solving Homogeneous Transform Equations of the Form AX = XB," *IEEE Trans. Robot. Autom.*, vol. 5, no. 1, pp. 16–29, 1989.

[18] J. S. Hu and Y. J. Chang, "Automatic Calibration of Hand-Eye-Workspace and Camera Using Hand-Mounted Line Laser," *IEEE/ASME Trans. Mechatronics*, vol. 18, no. 6, pp. 1778–1786, 2013.

[19] R. Y. Tsai and R. K. Lenz, "A New Technique for Fully Autonomous and Efficient 3D Robotics Hand/Eye Calibration," *IEEE Trans. Robot. Autom.*, vol. 5, no. 3, pp. 345–358, 1989.

[20] H. H. Chen, "A screw motion approach to uniqueness analysis of head-eye geometry," *IEEE CVPR*, pp. 145–151, 1991.

[21] J. C. Chou and M. Kamel, "Finding the position and orientation of a sensor on a robot manipulator using quaternions," *Int. J. Rob. Res.*, vol. 10, no. 3, pp. 240–254, 1991.

[22] K. Daniilidis, "Hand-Eye Calibration Using Dual Quaternions," *Int. J. Rob. Res.*, vol. 18, no. 3, pp. 286–298, 1999.

[23] H. Zhuang, Z. S. Roth, and R. Sudhakar, "Simultaneous robot/world and tool/flange calibration by solving homogeneous transformation equations of the form AX = YB," *IEEE Trans. Robot. Autom.*, vol. 10, no. 4, pp. 549–554, 1994.

[24] F. Dornaika and R. Horaud, "Simultaneous Robot-World and Hand-Eye Calibration," *IEEE Trans. Robot. Autom.*, vol. 14, no. 4, pp. 617–622, 1998.

[25] S. Gwak, J. Kim, and F. C. Park, "Numerical optimization on the Euclidean group with applications to camera calibration," *IEEE Trans. Robot. Autom.*, vol. 19, no. 1, pp. 65–74, 2003.

[26] Z. Zhao, "Simultaneous robot-world and hand-eye calibration by the alternative linear programming," *Pattern Recognit. Lett.*, vol. 0, pp. 1–7, 2018.

[27] K. Eckenhoff, P. Geneva, and G. Huang, "Closed-form Preintegration Methods for Graph-based Visual-Inertial Navigation," *Int. J. Rob. Res.*, no. X, pp. 1–22, 2017.

[28] S. Grzonka, A. Karwath, F. Dijoux, and W. Burgard, "Activity-based estimation of human trajectories," *IEEE Trans. Robot.*, vol. 28, no. 1, pp. 234–245, 2012.

[29] T. Qin, P. Li, and S. Shen, "VINS-Mono: A Robust and Versatile Monocular Visual-Inertial State Estimator," *IEEE Trans. Robot.*, vol. 34, no. 4, pp. 1004–1020, 2018.

[30] G. C. Calafiore, L. Carlone, and M. Wei, "A distributed technique for localization of agent formations from relative range measurements," *IEEE Trans. Syst. Man, Cybern.*, vol. 42, no. 5, pp. 1065–1076, 2012.

[31] X. S. Zhou and S. I. Roumeliotis, "Determining 3-D relative transformations for any combination of range and bearing measurements," *IEEE Trans. Robot.*, vol. 29, no. 2, pp. 458–474, 2013.

[32] L. Carlone, D. M. Rosen, G. Calafiore, J. J. Leonard, and F. Dellaert, "Lagrangian duality in 3D SLAM: Verification techniques and optimal solutions," *IEEE ICRA*, pp. 125–132, 2015.

[33] G. Grisetti, C. Stachniss, and W. Burgard, "Nonlinear constraint network optimization for efficient map learning," *IEEE Trans. Intell. Transp. Syst.*, vol. 10, no. 3, pp. 428–439, 2009.
[34] G. Grisetti, R. Kümmerle, C. Stachniss, and I. Introduction, "A Tutorial on Graph-Based SLAM," *IEEE Intell. Transp. Syst. Mag.*, pp. 31–43, 2010.
[35] L. Carlone, R. Tron, K. Daniilidis, and F. Dellaert, "Initialization techniques for 3D SLAM: A survey on rotation estimation and its use in pose graph optimization," *IEEE ICRA*, no. June, pp. 4597–4604, 2015.
[36] L. Carlone and A. Censi, "From angular manifolds to the integer lattice: Guaranteed orientation estimation with application to pose graph optimization," *IEEE Trans. Robot.*, vol. 30, no. 2, pp. 475–492, 2014.
[37] L. Carlone and G. C. Calafiore, "Convex Relaxations for Pose Graph Optimization with Outliers," *IEEE Robot. Autom. Lett.*, vol. 3, no. 2, pp. 1160–1167, 2018.
[38] D. M. Rosen, L. Carlone, A. S. Bandeira, and J. J. Leonard, "SE-Sync: A certifiably correct algorithm for synchronization over the special Euclidean group," *Int. J. Rob. Res.*, vol. 38, no. 2-3, pp. 95–125, 2019.
[39] J. Briales and J. Gonzalez-Jimenez, "Cartan-Sync: Fast and Global SE(d)-Synchronization," *IEEE Robot. Autom. Lett.*, vol. 2, no. 4, pp. 2127–2134, 2017.
[40] V. Joukov, J. Cesic, K. Westermann, I. Markovic, I. Petrovic, and D. Kulic, "Estimation and Observability Analysis of Human Motion on Lie Groups," *IEEE Trans. Cybern.*, vol. 50, no. 3, pp. 1321–1332, 2020.
[41] F. Thomas, "Approaching dual quaternions from matrix algebra," *IEEE Trans. Robot.*, vol. 30, no. 5, pp. 1037–1048, 2014.
[42] J. Wu, Y. Sun, M. Wang, and M. Liu, "Hand-eye Calibration: 4D Procrustes Analysis Approach," *IEEE Trans. Instrum. Meas.*, 2019.
[43] O. Özyeşil, N. Sharon, and A. Singer, "Synchronization over Cartan Motion Groups via Contraction," *SIAM J. Appl. Algebr. Geom.*, vol. 2, no. 2, pp. 207–241, 2018.
[44] Q. Ge, A. Varshney, J. P. Menon, and C.-F. Chang, "Double quaternions for motion interpolation," in *Proceedings of the ASME Design Engineering Technical Conference*, 1998.
[45] J. M. McCarthy and S. Ahlers, "Dimensional synthesis of robots using a double quaternion formulation of the workspace," in *Robotics Research*. Springer, 2000, pp. 3–8.
[46] M. Wang and A. Tayebi, "Hybrid Pose and Velocity-bias Estimation on SE(3) Using Inertial and Landmark Measurements," *IEEE Trans. Automat. Contr.*, vol. PP, no. 3, pp. 1–1, 2018.
[47] J. Wu, M. Wang, H. Fourati, M. Liu, and H. Li, "Generalized n-Dimensional Rigid Registration: Theory and Application," *IEEE Trans. Signal Process.*, 2019.
[48] A. Geiger, P. Lenz, C. Stiller, and R. Urtasun, "Vision meets robotics: The KITTI dataset," *Int. J. Rob. Res.*, vol. 32, no. 11, pp. 1231–1237, 2013.
[49] J. M. M. Montiel, "ORB-SLAM : a Versatile and Accurate Monocular," *IEEE Trans. Robot.*, vol. 31, no. 5, pp. 1–15, 2015.
[50] J. Saunderson, P. A. Passilo, and A. S. Willsky, "Semidefinite descriptions of the convex hull of rotation matrices," *SIAM J. Optim.*, vol. 25, no. 3, pp. 1314–1343, 2015.

Jin Wu (S'15-M'17) was born in May, 1994 in Zhenjiang, Jiangsu, China. He received the B.S. Degree from University of Electronic Science and Technology of China, Chengdu, China. He has been a research assistant in Department of Electronic and Computer Engineering, Hong Kong University of Science and Technology (HKUST), since 2018, and is currently a PhD student with Robotics and Multi-Perception Lab (RAM-LAB), HKUST, under the supervision of Prof. Ming Liu. His research interests include robot navigation, multi-sensor fusion, mechatronics, and circuitization of robotic applications. He is a co-author of over 50 technical papers in representative journals and conference proceedings of IEEE, AIAA, IET and etc. One of his papers published in IEEE TRANSACTIONS ON AUTOMATION SCIENCE AND ENGINEERING was selected as the ESI Highly Cited Paper by ISI Web of Science during 2017 to 2018. He is a member of IEEE.

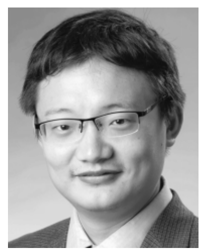

Ming Liu (S'12-M'13-SM' 18) received the B.A. degree in automation from Tongji University, Shanghai, China, in 2005, and the Ph.D. degree from the Department of Mechanical and Process Engineering, ETH Zurich, Zurich, Switzerland, in 2013, supervised by Prof. Roland Siegwart. During his master's study with Tongji University, he stayed one year with the Erlangen-Nunberg University and Fraunhofer Institute IISB, Erlangen, Germany, as a Master Visiting Scholar.

He is currently with the Electronic and Computer Engineering, Computer Science and Engineering Department, Robotics Institute, The Hong Kong University of Science and Technology (HKUST), Hong Kong, China, as an Associate Professor. He is also a founding member of Shanghai Swing Automation Ltd., Co. He is currently the chairman of Shenzhen Unity Drive Inc., China. He is coordinating and involved in NSF Projects and National 863-Hi-TechPlan Projects in China. His research interests include dynamic environment modelling, deep-learning for robotics, 3-D mapping, machine learning, and visual control.

Dr. Liu was a recipient of the European Micro Aerial Vehicle Competition (EMAV'09) (second place) and two awards from International Aerial Robot Competition (IARC'14) as a Team Member, the Best Student Paper Award as first author for MFI 2012 (IEEE International Conference on Multisensor Fusion and Information Integration), the Best Paper Award in Information for IEEE International Conference on Information and Automation (ICIA 2013) as first author, the Best Paper Award Finalists as co-author, the Best RoboCup Paper Award for IROS 2013 (IEEE/RSJ International Conference on Intelligent Robots and Systems), the Best Conference Paper Award for IEEE CYBER 2015, the Best Student Paper Finalist for RCAR 2015 (IEEE International conference on Real-time Computing and Robotics), the Best Student Paper Finalist for IEEE ROBIO 2015, the Best Student Paper for IEEE ROBIO 2019, the Best Student Paper Award for IEEE ICAR 2017, the Best Paper in Automation Award for IEEE ICIA 2017, twice the innoviation contest Chunhui Cup Winning Award in 2012 and 2013, and the Wu Wenjun AI Award in 2016. He was the Program Chair of IEEE RCAR 2016 and the Program Chair of International Robotics Conference in Foshan 2017. He was the Conference Chair of ICVS 2017. He has published many popular papers in top robotics journals including IEEE TRANSACTIONS ON ROBOTICS and *International Journal of Robotics Research*. Dr. Liu is an Associate Editor of IEEE ROBOTICS AND AUTOMATION LETTERS, *IET Cyber-Systems and Robotics*, *International Journal of Robotics and Automation*. He is a Senior Member of IEEE.

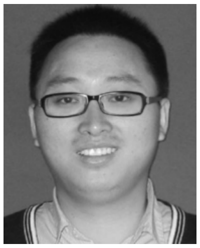

Yulong Huang (M'19) received the B.S. degree in Automation from the College of Automation, Harbin Engineering University, Harbin, China, in 2012. He received the Ph.D degree in control science and engineering from the College of Automation, Harbin Engineering University, Harbin, China, in 2018. From Nov. 2016 to Nov. 2017, he was a visiting graduate researcher at the Electrical Engineering Department of Columbia University, New York, USA. Currently, he is an Associate Professor of navigation, guidance, and control in Harbin Engineering University (HEU) in China.

From Dec. 2019 to Dec. 2021, he will be associated with the Department of Mechanical Engineering, City University of Hong Kong, as a Hong Kong Scholar. His current research interests include signal processing, information fusion and their applications in navigation technology, such as inertial navigation and integrated navigation. He is the recipient of excellent doctoral thesis from Chinese Association of Automation (CAA) in 2019.

Chi Jin was born in Shanghai, China, in 1989. He received the B.S. degree in mechanical engineering from Tongji University, Shanghai, China, in 2012. In 2017, he received the Ph.D. degree in automatic control at the Laboratory of Signals and Systems, Centrale- Supelec-CNRS-Universite Paris Sud, Gif-sur-Yvette, France.

His research interests include time-delay systems, and nonlinear control with applications to automotive vehicles and robotics. He is currently working as a Senior Research Scientist in DJI Innovations Inc., Shenzhen, China.

Yuanxin Wu (SM'14) received the B.Sc. and Ph.D. degrees in navigation from the Department of Automatic Control, National University of Defense Technology, Changsha, China, in 1998 and 2005, respectively.

From 2006 to 2007, he was a Lecturer with National University of Defense Technology, where from 2008 to 2012, he was an Associate Professor, from 2009 to 2010, he was a visiting Postdoctoral Fellow with the Department of Geomatics Engineering, University of Calgary, Calgary, Canada, and from 2013 to 2015, he was a Professor with the Central South University, Changsha, China. He is currently a Professor with the School of Electronic Information and Electrical Engineering, Shanghai Jiao Tong University, Shanghai, China. His current research interests include inertial-based navigation system, state estimation, inertial-visual fusion, and wearable human motion sensing.

He was the recipient of the National Excellent Doctoral Dissertation in 2008, New Century Excellent Talents in University in 2010, Fok Ying Tung Education Fellowship in 2012, NSFC Award for Excellent Young Scientists in 2014, Natural Science and Technology Award in University in 2008 and 2016, and Elsevier's Most Cited Chinese Researchers (Aerospace Engineering) from 2015 to 2017. He serves as an Associate Editor for *The Journal of Navigation* and IEEE Transactions on Aerospace and Electronic Systems.

Changbin Yu (M'08–SM'10) was born in Shandong, China in 1981. He received the B.Eng. degree with first class honors in computer engineering from Nanyang Technological University, Singapore, in 2004, and the Ph.D. degree in engineering from the Australian National University (ANU), Canberra, Australia, in 2008.

Since 2008, he has been a faculty member with the Research School of Engineering, ANU. He obtained tenure with ANU in 2014 and still holds an Honorary Professorship. In 2017, he founded the AI and Robotics Centre, Westlake University, Hangzhou, China. He was appointed as the Optus Chair to establish the Optus-Curtin Centre of Excellence in AI, Curtin University, Perth, WA, Australia.

Dr. Yu was a recipient of the 2010 ANU Top Supervisor Award, the 2006–2008 Asian Journal of Control Best Paper Award, the ARC Australian Postdoctoral Fellowship in 2007, the Queen Elizabeth II Fellowship in 2010, the 2006 Chinese Government Award for Outstanding Students Abroad, and the 2005 Australian Government's Endeavor Asia Award. He is a Fellow of the Institution of Engineers Australia and a Member of IFAC Technical Committee on Networked Systems. He served as a Subject Editor for the International Journal of Robust and Nonlinear Control and was an Associate Editor for the System & Control Letters and IET Control Theory & Applications.